Structures that accommodated differential vertical axis rotation of the western Transverse Ranges, California

Nathan W. Onderdonk[1]

Department of Geological Sciences, University of California, Santa Barbara, California, USA

Received 13 November 2004; revised 11 April 2005; accepted 17 May 2005; published 27 August 2005.

[1] New paleomagnetic and structural data from the northwestern Transverse Ranges of California define the location, geometry, and kinematics of structures that facilitated differential vertical axis rotation. Paleomagnetic declinations in the southern Coast Ranges indicate negligible amounts of vertical axis rotation, which contrasts sharply with data from rocks of the same age in the western Transverse Ranges that record approximately 90° of clockwise rotation since early Miocene time. This change in paleomagnetic declinations occurs across an east-west trending zone of reverse faults and folds that includes the western Big Pine–Pine Mountain fault, the Santa Ynez fault, and the structures in between. The structures in this zone exhibit increased amounts of shortening to the west such that the zone closed in a fan-like fashion, resulting in rotation of the southern edge with respect to the northern edge. The new data and interpretations refine previous models of vertical axis rotation in southern California by describing the deformation present at rotation boundaries that allowed distinct areas to rotate relative to the surrounding crust.
Citation: Onderdonk, N. W. (2005), Structures that accommodated differential vertical axis rotation of the western Transverse Ranges, California, *Tectonics*, *24*, TC4018, doi:10.1029/2004TC001769.

1. Introduction

[2] Abundant paleomagnetic data from volcanic and sedimentary rocks in the western Transverse Ranges (WTR) of southern California indicate that this area (Figure 1) rotated clockwise approximately 90° since early Miocene time [e.g., *Kamerling and Luyendyk*, 1979, 1985; *Hornafius et al.*, 1986; *Liddicoat*, 1990; *Luyendyk*, 1991]. The paleomagnetic data are consistent with anomalous east-west structural and stratigraphic trends in the WTR and the apparent dislocation of older regional lithologic belts [*Jones et al.*, 1976; *Hamilton*, 1978; *Crouch*, 1979]. *Luyendyk et al.* [1980] proposed a geometric model to explain the kinematics of large-magnitude rotation of the WTR that has since been refined and expanded by subsequent models [*Luyendyk*, 1991; *Crouch and Suppe*, 1993; *Nicholson et al.*, 1994; *Dickinson*, 1996]. These models propose that clockwise rotation of crustal blocks occurs along left-lateral strike-slip (or oblique slip) faults while nonrotating crust to the north and south slip out of the way along right-lateral faults. A key requirement of these models is that they satisfy the observation that crust to the north and south of the rotated domain does not show evidence of significant rotation.

[3] Although these models appear to fit the regional kinematic framework of southern California, the specific manner in which differential rotation is accommodated at boundaries between rotated and nonrotated crust has not been completely resolved. Most current models [e.g., *Luyendyk*, 1991; *Crouch and Suppe*, 1993; *Nicholson et al.*, 1994] imply complex kinematics along rotation boundary faults that have not been verified by direct field observations. For example, *Dickinson* [1996] presents geometric models of rotation that show significant overlaps and holes along the rotation domain boundaries such that these boundaries must exhibit primarily dip-slip displacement with considerable variations along strike. However, his proposed regional reconstruction assigns these boundaries to faults that he cites as exhibiting only left-lateral strike slip. The models assume that space problems at the boundaries are partly accommodated by block-internal deformation, which has not been documented. In addition, the specific locations of the rotation boundary faults in these models have been inferred from regional structural trends and were not fully supported by observed contrasts in paleomagnetic data.

[4] Crucial to understanding how large-magnitude vertical axis rotation is accomplished in the brittle crust is knowing where the rotation boundaries are, what kind of deformation occurs at rotation boundaries, and the spatial extent over which this deformation is distributed. These characteristics are important details that hold significant implications for the mechanics of vertical axis rotation and therefore need to be incorporated into the regional models. In this paper I present new paleomagnetic and structural data that define the specific location, structural framework, and kinematics of a rotation boundary in southern California. I evaluate the implications of these new data and suggest adjustments to the existing models.

2. Geologic Setting

[5] This research was conducted along the northern edge of the western Transverse Ranges (WTR), located at the Pacific-North American plate boundary adjacent to the San

[1]Now at Physics of Geological Processes, University of Oslo, Oslo, Norway.

0278-7407/05/2004TC001769$12.00

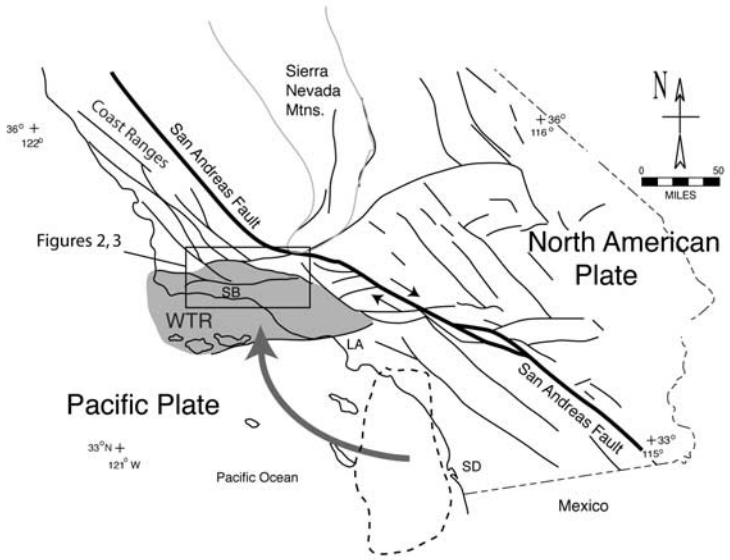

Figure 1. Fault map of southern California (modified from Figure 2 of *Luyendyk* [1991]) showing the main plate boundary (San Andreas fault) between the Pacific Plate and the North American Plate and showing inferred Neogene clockwise rotation of the western Transverse Ranges domain (shaded area). The dashed outline shows the approximate prerotational orientation of the western Transverse Ranges (WTR). Note that contemporaneous translations of other crustal blocks are not portrayed (refer to Figure 3 of *Nicholson et al.* [1994] for a complete description of crustal movements). Santa Barbara (SB), Los Angeles (LA), and San Diego (SD) are shown for reference.

Andreas fault in southern California (Figure 1). The present-day geology of the region is the result of a complex history of tectonic events that occurred along the western edge of North America. The evolution of a transform boundary along the western edge of North America since 28 Ma [*Atwater*, 1989; *Lonsdale*, 1991] has resulted in the dislocation, translation, and rotation of previously northwest trending lithologic belts that formed during Mesozoic and early Tertiary subduction. Part of this disrupted lithologic belt is present in the WTR where a thick sequence of Jurassic through Eocene forearc sedimentary rocks overlies continental arc basement rocks and an accretionary wedge complex (Franciscan formation). The juncture of these two basement terranes is concealed beneath the sedimentary sequence, so its exact nature and location in the WTR is unknown. Late Tertiary sedimentary and volcanic rocks lie on top of the forearc basin sequence (Figure 2) and consist of terrestrial Oligocene deposits overlain by mostly marine rocks of Miocene to Pleistocene age [*Dibblee*, 1982].

[6] Tectonic structures within the WTR are mainly east-west striking faults and folds. Most of these faults exhibit reverse and some left-lateral strike-slip displacement and many are currently active. The Santa Ynez fault (Figure 2) is one of the largest structures in the northern WTR and has lifted the Santa Ynez and Topa Topa ranges (Figure 3) to altitudes of more than 2000 m. North of this fault is a westward widening zone of reverse faults and folds, separated from the Santa Maria basin to the west by the Little Pine fault. The northern edge of this zone is bounded by the Pine Mountain and western Big Pine faults, both of which are north dipping thrust faults with 2000 m high mountain ranges in their hanging walls.

[7] The southern Coast Ranges to the north are composed of roughly the same forearc sedimentary rocks and underlying basement terranes found in the WTR. These are overlain by late Cenozoic sedimentary and volcanic rocks that are also similar to rocks of the same age in the WTR, although there are significant stratigraphic differences between the two regions [*Onderdonk*, 2003]. The rocks in the southern Coast Ranges are deformed by northwest trending folds and faults. Most of the faults exhibit reverse and/or right-lateral strike-slip displacement. All of these northwest trending structures are truncated at their southern ends by the east-west faults of the WTR.

[8] Paleomagnetic declinations reported from within the WTR are deflected 75° to 90° clockwise in sedimentary units of the Santa Ynez and Topa Topa ranges [e.g., *Hornafius*, 1985; *Liddicoat*, 2001] and more than 90° in the volcanic rocks of the Channel Islands and Santa Monica Mountains [*Kamerling and Luyendyk*, 1979, 1985]. Prior to this study, the boundaries of the rotated domain were not accurately defined by paleomagnetic contrasts, due to a lack of paleomagnetic sampling directly north and south of the WTR. Rotation of the WTR began about 18 Ma [*Hornafius et al.*, 1986] and has continued to the present [*Luyendyk*, 1991]. Regional geologic relationships and correlations along the south side of the rotated domain indicate that

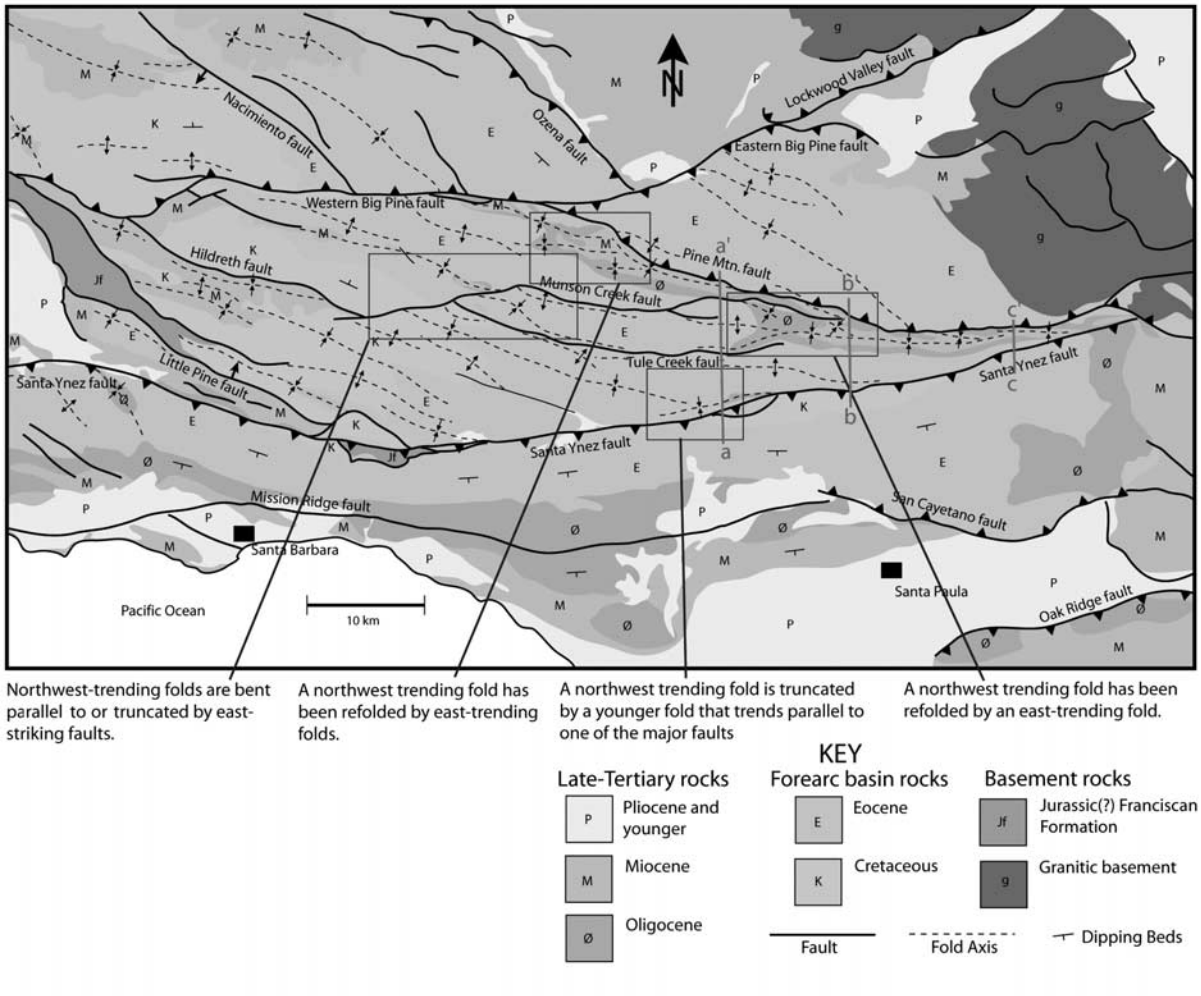

Figure 2. Geologic map of the northwestern Transverse Ranges showing fold orientations and locations of cross sections (a-a′, b-b′, c-c′ in Figure 6). Compiled from *Dibblee* [1985] and *Dibblee and Ehrenspeck* [1986, 1987a, 1987b, 1987c, 1988], *Jennings et al.* [1977], and *Onderdonk* [2003]. See color version of this figure in the HTML.

the early Miocene and older rocks in the WTR were originally oriented north-south adjacent to rocks exposed along the coast of San Diego (Figure 1) [*Yeats et al.*, 1974; *Kamerling and Luyendyk*, 1979, 1985]. The presence of the Los Angeles basin and geologic features of the inner California borderland imply that the WTR rotated clockwise about a pivot point at its east end while translating to the northwest along the plate boundary [*Luyendyk et al.*, 1980; *Crouch and Suppe*, 1993; *Nicholson et al.*, 1994].

3. Field and Laboratory Procedures

[9] Geologic mapping was conducted at a scale of 1:16,000 along a 30 km stretch of the Pine Mountain and Big Pine faults, centered on the area where these two faults intersect (Figure 2). Mapping was accompanied by structural investigations and the collection of kinematic data from fault exposures throughout most of the northwestern Transverse Ranges and southern Coast Ranges. The new data and mapping were analyzed in parallel with previously published maps and used to evaluate the style and magnitude of regional deformation.

[10] Paleomagnetic samples were collected from sedimentary and volcanic rocks at 27 sites in the northwestern Transverse Ranges and southern Coast Ranges. The locations were chosen to fill gaps in previously reported data and to define the northern extent of the highly rotated domain. The sedimentary rocks sampled include Late Cretaceous, Eocene, and Oligocene fine-grained sandstone and shale. The volcanic rocks sampled include early Miocene basaltic flows and pillow basalts, and late Oligocene rhyolite dikes. All of the rocks sampled formed before or during the inception of rotation and thus the paleomagnetic data obtained from these rocks record the full Miocene to present rotation amount at each site.

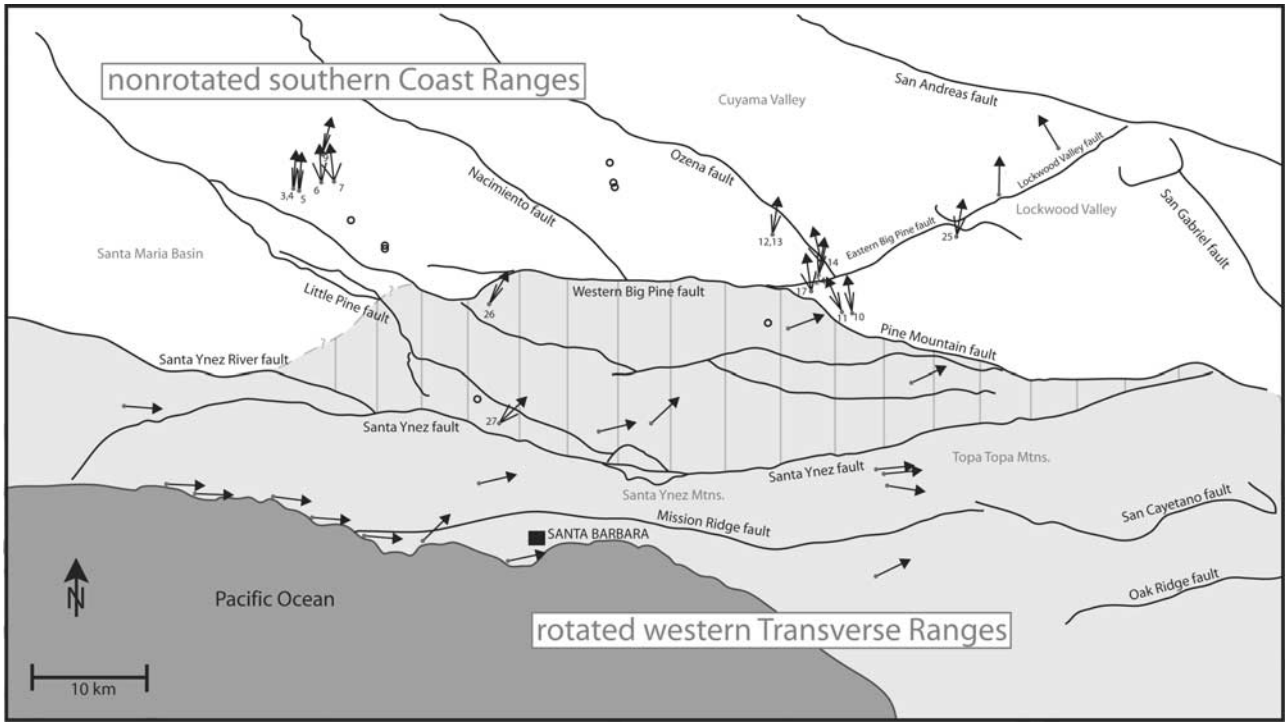

Figure 3. Map of paleomagnetic data (arrows) and major faults of the northwestern Transverse Ranges (see Figure 1 for location). The extent of the rotated western Transverse Ranges domain (shaded), the transition zone (vertical lines), and the nonrotated crust of the southern Coast Ranges (white area) are shown. Arrows represent declination directions for samples collected from Miocene and pre-Miocene sedimentary and volcanic rocks. Sites with error bars and locality numbers represent paleomagnetic data collected during this study. Other sites represent previously published data [*Kamerling and Luyendyk*, 1979; *Terres*, 1984; *Hornafius*, 1985; *Liddicoat*, 1990; *Whidden*, 1994; *Prothero and Britt*, 1998]. Open circles represent sampled locations that did not yield acceptable data due to overprinting, weak magnetization, or large α_{95}.

[11] Sample cores were collected in the field using a gas-powered diamond drill and were oriented with a Brunton compass attached to a nonmagnetic orienting sleeve. Bedding attitude was measured and used to obtain tilt-corrected directions. As large an outcrop area as possible was sampled at each site to analyze multiple beds in the sedimentary rocks, multiple flows in the volcanic rocks, and a range of inner and outer edge portions of the intrusive rocks. The samples were then measured using the 2G Cryogenic Magnetometer at the California Institute of Technology. A combination of alternating field and thermal demagnetization techniques were used on every sample. After measuring the natural remanent magnetism of each sample, they were subjected to stepwise alternating field demagnetization in eight steps to 200 mT. Samples were then thermally demagnetized in 50°C steps from 150°C to roughly 450°C. Because of variations in the intensity and stability of the characteristic remnant magnetism (ChRM) in each rock type sampled, different amounts and increments of further thermal demagnetization were employed above 450°C.

[12] The volcanic rock samples showed strong stable directions with no present-day field overprint (Figure 4). All the early Miocene basalt samples, from four different sites, exhibited reversed polarity (Table 1). Primary directions for volcanic rock samples were determined by constructing a best fit line from the origin through consecutive points on vector projection diagrams.

[13] All of the sedimentary samples exhibited a normal, present-day field overprint at the lower demagnetization levels. Progressive demagnetization resulted in successive total magnetization vectors that moved away from the present-day field direction toward either a reversed polarity direction or a tilt-corrected normal polarity direction. The arcs prescribed by the successive directions were fit to circles and the interpreted primary direction was obtained using the plane conversion techniques originally proposed by *Halls* [1976] and *Hoffman and Day* [1978] (Figure 4). Statistical techniques following the methods outlined by *McFadden and McElhinny* [1988] were used for sites where both plane conversion and stable endpoint techniques were applied to different samples. The sedimentary samples that exhibited nonrotated normal directions were accepted only if the present-day field direction at low temperatures was statistically different from the interpreted ChRM direction. Samples that did not satisfy

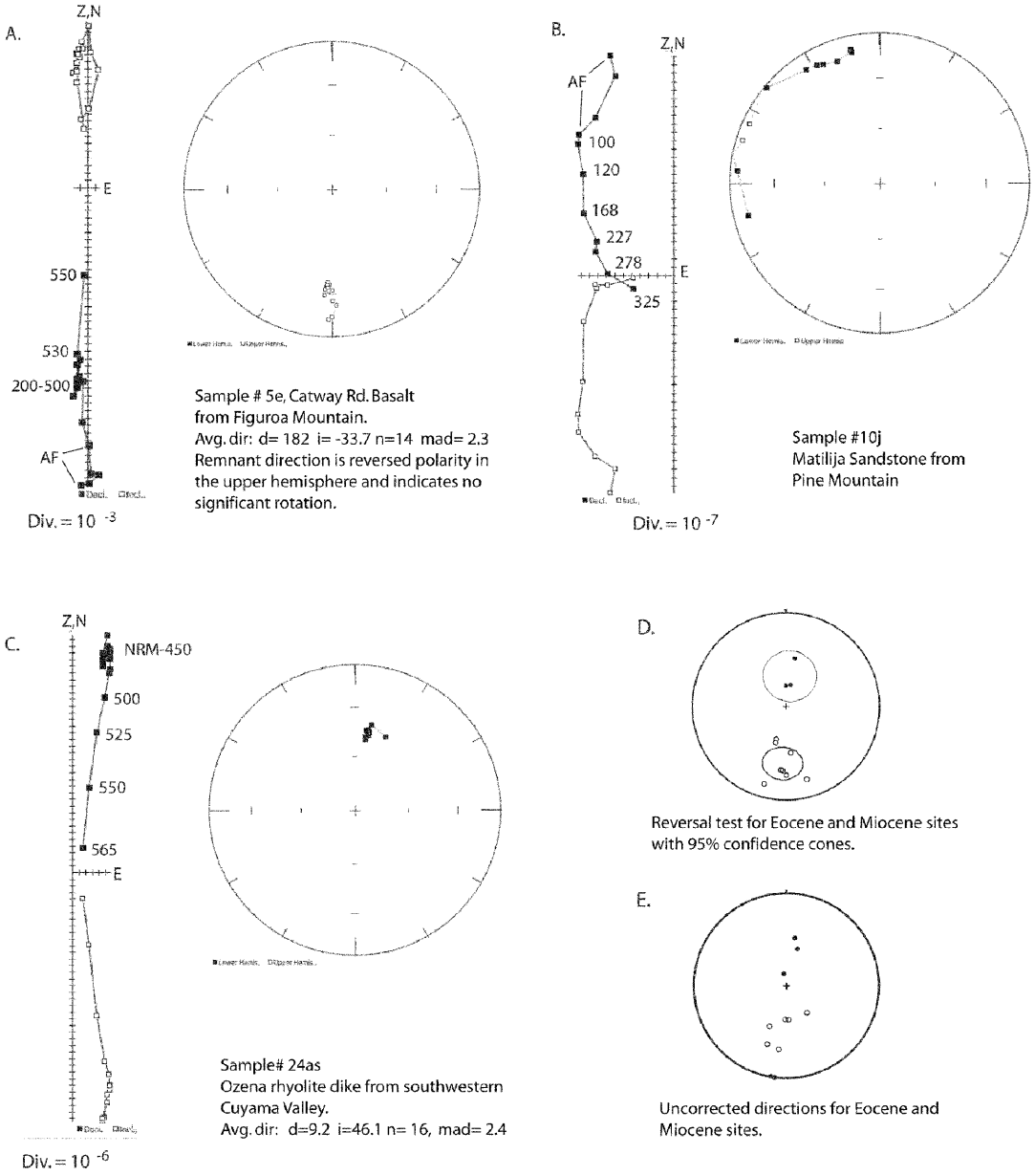

Figure 4. (a, b, c) Zijderveld and equal-area diagrams showing progressive demagnetization data from typical sedimentary and intrusive rock samples. (d) Reversal test. (e) Directions before tilt correction. MAD, maximum angular deviation.

this condition were disregarded because the possibility of complete overprinting by the present-day field could not be confidently eliminated.

[14] A Fisher distribution was used to calculate site mean statistics and error estimates for each site (Table 1). Ten of 27 sites were rejected due to high errors in sample directions, typically associated with low intensities or complete overprinting in sedimentary rock samples, that prevented the determination of an original magnetization direction. Standard tilt corrections were performed for each site. Plunge corrections were also done for three sites (10,11,17) which showed less than a 6° difference between the end-members of plunge correction possibilities. The Eocene and Miocene site means passed a reversal test (Figure 4), but the sites were not established in locations suitable for a fold test. For the volcanic rock sites, secular variation cannot be fully evaluated due to the scarcity and isolated nature of volcanic rocks in the

Table 1. Paleomagnetic Data From Selected Areas in the Northwestern Transverse Ranges and Southern Coast Ranges[a]

Site	Location	Latitude, Longitude	Strike/ Dip	Rock Type	Age	Method	α_{95}	N	D, deg	I, deg	Amount of Rotation, deg	Error Angle, deg	Amount of Flattening, deg
					Nonrotated Sites								
3,4	Figueroa Mountain	34°45.41, 119°59.19	120°/35°S	basalt	18.8 Ma	stable endpoint	7.4	8	186	−32	5.4	10.4	26.2
5	Figueroa Mountain	34°45.11, 119°58.89	120°/35°S	basalt	18.8 Ma	stable endpoint	3.5	9	183	−32	1.9	7.0	26.3
6	Manzana Creek	34°46.33, 119°56.77	110°/35°N	ss	Cretaceous	plane conversion and stable endpoint	16.0	9	18	26	−3.8	18.0	30.8
7	Manzana Creek	34°46.17, 119°56.22	125°/62°N	sh	Cretaceous	plane conversion and stable endpoint	27.0	5	195	−12	−6.8	28.0	44.8
9	Hurricane Deck	34°47.61, 119°57.46	125°/50°N	Vaqueros ss	lower Miocene	plane conversion	4.0	10	196	−15	14.9	7.0	43.5
10	Pine Mountain	34°38.40, 119°20.06	88°/33°N	Matilija ss	Eocene	plane conversion	5.0	10	180	−27	−8.4	7.5	34.2
11	Pine Mountain	34°38.44, 119°20.63	95°/46°N	Matilija ss	Eocene	plane conversion	8.0	6	164	−20	−24.4	9.9	41.2
12,13	Tinta Creek	34°42.99, 119°25.34	133°/10°S	Juncal ss	Eocene	plane conversion and stable endpoint	5.0	10	197	−60	8.6	11.0	1.3
14	Cuyama River	34°41.23, 119°21.83	133°/23°S	Juncal sh	Eocene	plane conversion	10.0	8	174	−49	−14.4	16.0	12.3
15	Cuyama River	34°41.20, 119°21.81	115°/23°S	Juncal sh	Eocene	plane conversion	16.0	7	195	−57	6.6	30.8	4.3
17	Pine Mountain	34°40.69, 119°22.14	125°/18°S	Matilija ss	Eocene	stable endpoint	5.8	5	0	72	−8.4	19.7	−10.0
24	Ozena	34°40.60, 119°21.79	170°/90°	rhyolite dike	25.2 to >25 Ma	stable endpoint	5.0	9	10	46	8.9	9.0	12.0
25	Wagon Road Canyon	34°42.61, 119°12.36	130°/80°S	rhyolite dike	25.2to >25 Ma	stable endpoint	4.2	9	12	71	10.9	14.0	−12.0
Mean							11.7	13	187	−40			
					Transition Zone Sites								
26	Flores Flat	34°39.04, 119°45.37	90°/37°S	diabase sill	lower Miocene	stable endpoint	4.4	9	211	−38	30.2	8.0	20.0
27	Santa Ynez River	34°31.88, 119°43.60	107°/58°N	Sespe sh	Oligocene	stable endpoint	17.8	4	50	17	45.9	19.0	42.4

[a]N, number of samples; D, declination; I, inclination; ss, sandstone; sh, shale. Sites 1, 2, 8, 16, 18, 19, 20, 23, 28, 29 have data too poor (due to high errors, weak magnetizations, or complete overprinting) to obtain primary direction. Primary directions were determined using the methods of *Kirschvink* [1980]. Rotation and error were calculated using the method of *Beck* [1980] with *Demarest*'s [1983] correction. Reference poles used were as follows: *Calderone et al.* [1990], latitude 85.5°, longitude 108.9°, α_{95}: 4.4, age Miocene; *Diehl et al.* [1983], latitude 83.2, longitude 148.0, α_{95} 4.1, age Oligocene; *McElhinny and McFadden* [2000], latitude 80.0, longitude 158.0, α_{95} 3.7, age Eocene; *McElhinny and McFadden* [2000], latitude 72.3, longitude 194.8, α_{95} 3.7, age Late Cretaceous.

area. The data from these sites are considered valid because their directions agree with results from nearby sedimentary sites.

[15] The magnitude of rotation, flattening, and angular error for each sample site was calculated using the method of *Beck* [1980] and are displayed in Table 1. Many of the sample sites exhibited inclinations that are significantly shallower than expected at the present latitude. The anomalous inclinations are most likely due in part to compaction processes in the sedimentary rocks [*Arason and Levi*, 1990] and possibly related to secular variation in the volcanic rocks. Shallow inclinations are also a common characteristic of Mesozoic and Cenozoic rocks in the region that has been reported by many studies [e.g., *McWilliams and Howell*, 1982; *Champion et al.*, 1984; *Liddicoat*, 1990; *Prothero and Britt*, 1998]. The specific cause of the regional inclination flattening is a subject of debate (discussed by *Lund et al.* [1991]).

4. Results

4.1. Definition of the Rotation Boundary by Paleomagnetic Data

[16] The paleomagnetic results of this study show no significant systematic rotation in the southern Coast Ranges. Declinations are within 15° of the expected direction with approximately equal amounts of clockwise and counterclockwise deviation (Figure 3). This result agrees with previously reported paleomagnetic data from adjacent areas [e.g., *Terres*, 1984] and the lack of rotation predicted for the southern Coast Ranges by kinematic models and regional

reconstructions [e.g., *Luyendyk*, 1991; *Crouch and Suppe*, 1993]. The absence of rotation in this area differs significantly from the Santa Ynez and Topa Topa ranges of the WTR, 20 km to the south, where an average of 90° of clockwise rotation is indicated by previously reported paleomagnetic data (Figure 3). Differential rotation has therefore occurred between these two areas and the contrasts in paleomagnetic declination constrain the location of the rotation boundary.

[17] Between these contrasting domains, previously reported paleomagnetic data and two site locations from this study define an intermediate zone where declinations are rotated an average of 51°, ranging from 30° to 75°. These data indicate that the rotation boundary is not a single fault, but a transition zone between the highly rotated and nonrotated crust. This rotation boundary zone, as defined by the paleomagnetic data, consists of the area between the western Big Pine-Pine Mountain fault on the north and the Santa Ynez fault on the south.

4.2. Structural Framework and Kinematics of the Rotation Boundary

[18] Structural data and detailed mapping along the Big Pine and Pine Mountain faults show that the western Big Pine fault is a north dipping thrust fault that is continuous with the Pine Mountain thrust. This major structure, herein designated as the ''western Big Pine–Pine Mountain fault,'' truncates the eastern Big Pine fault, which dips to the south and exhibits south-side-up displacement (Figure 5). This structural relationship is a key observation that significantly adjusts the structural framework and kinematics of the region. The previous interpretation of a single continuous ''Big Pine fault'' exhibiting late Cenozoic strike-slip displacement [*Hill and Dibblee*, 1953] is not supported by the results of this study (see Appendix A).

[19] The western Big Pine-Pine Mountain fault (WBP-PM fault) delineates the northern edge of the rotation boundary zone (Figure 3). The fault dips 30° to 50° to the north and exhibits reverse displacement, putting Late Cretaceous and Eocene rocks in the hanging wall over tightly folded overturned synclines of Eocene through Pliocene rocks in the footwall (Figure 2). Exposures of the fault show a 5 to 25 m wide zone of gouge, intensely sheared rock, and phacoids of hanging wall rocks. Kinematic indicators such as gouge fabric, rare slickensides, drag folds, and tight z and s folds present at various scales in the fault zone indicate primarily reverse displacement. Attempts to quantify displacement on the fault were unsuccessful. Abrupt changes across the fault in Eocene unit thicknesses, Miocene through Pliocene stratigraphy, and structural orientations make precise restoration impossible [*Onderdonk*, 2003]. These differences across the fault vary along strike. Estimates of dip-slip separation typically increase to the west, but this pattern is disrupted where the WBP-PM fault truncates structures of the southern Coast Ranges. Cross sections constructed along the eastern half of the fault demonstrate the apparent westward increase in dip-slip displacement as the fault thrusts Eocene rocks in the hanging wall progressively farther over a sequence of folds in the footwall (Figure 6). *Gordon* [1978] also reported a westward increase in dip-slip along the fault in this area and noted that the slip decreases to almost zero at its east end. This differs from the western end of the fault where no decrease in displacement is observed and the fault bends to the northwest (Figure 3).

[20] The southern edge of the rotation boundary zone is marked by the Santa Ynez fault (Figure 3). The Santa Ynez fault is a major east-west striking fault that dips to the south along most of its length and exhibits reverse displacement that has lifted up the Santa Ynez and Topa Topa ranges along its south side. The fault puts lower Eocene and Late Cretaceous rocks in the hanging wall over Eocene through Miocene rocks in the footwall. Exposures of the fault typically show a 10 to 20 m wide zone of gouge and sheared rock. As with the WBP-PM fault, a quantitative determination of displacement across the Santa Ynez fault is not possible due to a change in structural grain across the fault (Figure 2). Cross sections along the eastern part of the fault, however, suggest a westward increase in dip-slip separation. The stratigraphic separation also decreases to zero at its east end where the fault is truncated by the WBP-PM fault (Figure 2). Slip estimates cannot be inferred from cross sections farther west along the central Santa Ynez fault due to increased differences in structural grain across the fault. Along the western part of the fault in the Santa Maria basin, displacement is transferred to the Santa Ynez River fault [*Sylvester and Darrow*, 1979], which has been interpreted to be a major structural boundary from geophysical evidence [*Up de Graff and Luyendyk*, 1989], stratigraphic contrasts [*Dibblee*, 1982], and paleomagnetic contrasts [*Hornafius*, 1985].

[21] In addition to significant dip-slip offset, the Santa Ynez fault is also assumed to have experienced left-lateral strike-slip displacement [*Dibblee*, 1982]. This hypothesis is supported by kinematic data collected along the fault during this study (Figure 7). Attempts to determine the amount of strike-slip displacement across the fault based on various lithologic correlations has resulted in conflicting reports that vary from 3 km [*Link*, 1971] to 60 km [*Edwards*, 1971]. After analysis of these and other reported correlations [e.g., *McCracken*, 1972; *McCulloh*, 1981], it is my opinion that none of them is unique enough to constrain an accurate determination of strike-slip offset.

[22] Between the WBP-PM fault and the Santa Ynez fault is a westward opening zone of reverse faults and folds. The Munson Creek and Tule Creek faults are the larger faults in this zone. Both faults dip steeply south except where they are folded by the WBP-PM fault at their east ends. These faults exhibit reverse displacement with larger amounts of dip-slip displacement to the west as indicated by increased offsets of Eocene contacts. As a result, the total dip-slip separation across the faults varies along strike with maximum amounts of approximately 2 km on the Tule Creek fault and about 1 km on the Munson Creek fault. Kinematic indicators collected along these faults show evidence of

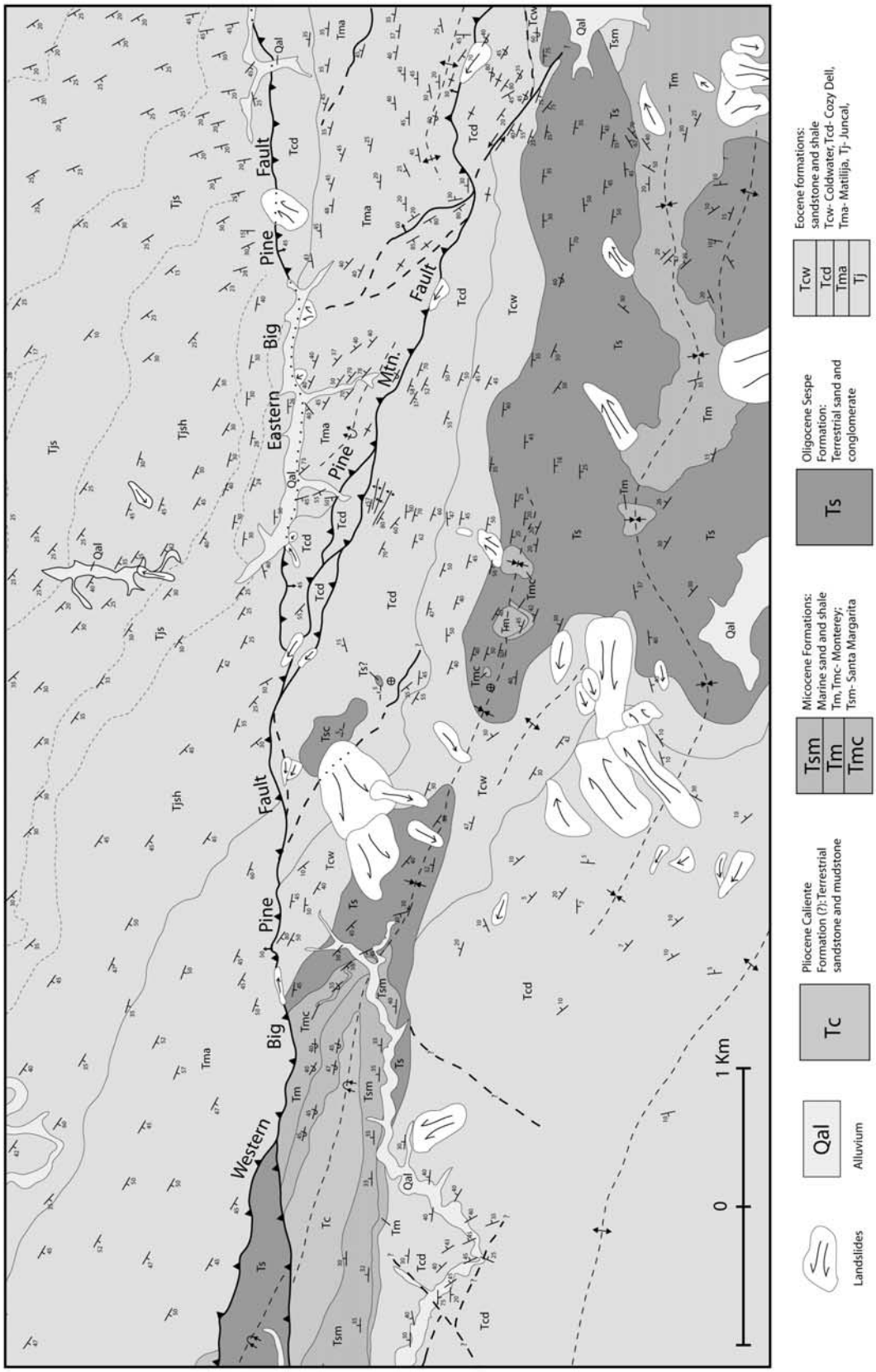

Figure 5. Simplified geologic map from the southern Rancho Nuevo Creek quadrangle showing the juncture between the WBP-PM fault and the eastern Big Pine fault.

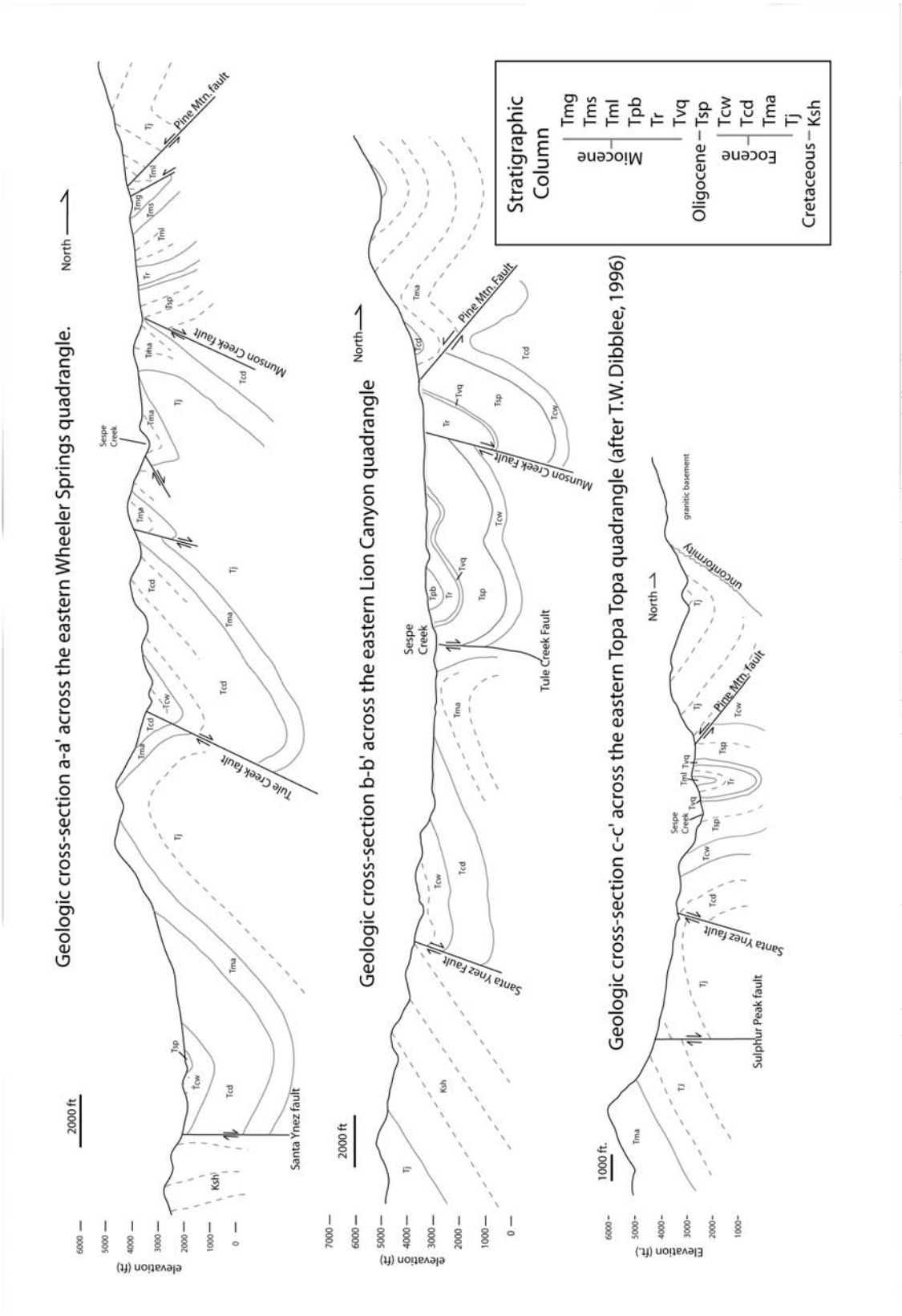

Figure 6. Geologic cross sections across the rotation boundary zone showing increased dip-slip separation westward on the Pine Mountain and Santa Ynez faults. Folds in the bottom (eastern) cross sections are progressively thrust under the Pine Mountain fault to the west. Refer to Figure 2 for locations of cross sections.

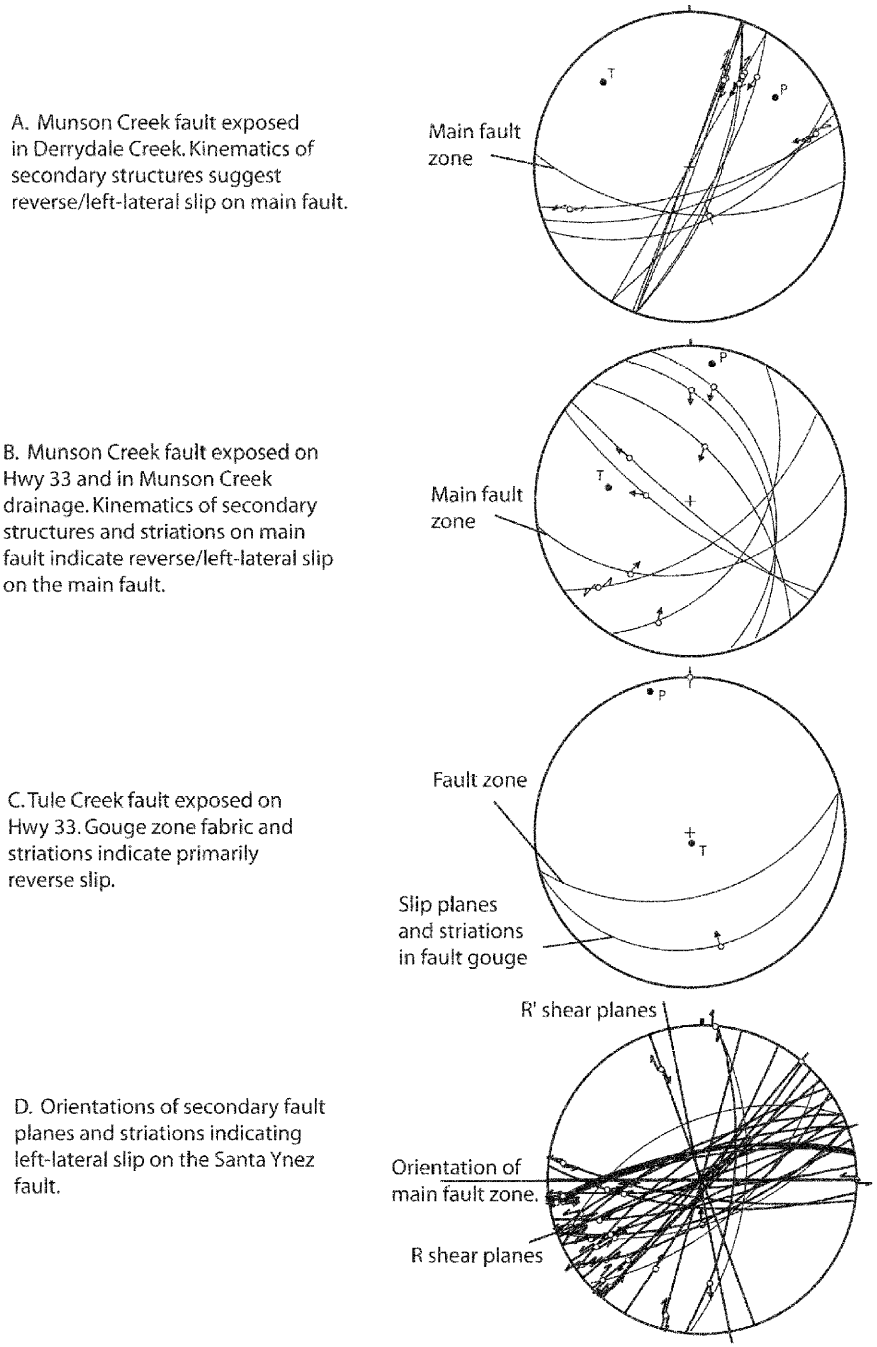

Figure 7. Stereograms of kinematic indicators collected along boundary zone faults. Fault planes are projected on lower hemisphere. Double arrows show strike-slip displacements, and single arrows indicate motion of hanging wall. Tension (T) and pressure (P) axes are also shown.

primarily reverse slip with a slight component of left-lateral strike slip (Figure 7).

[23] Most of the map-scale folds in the boundary zone trend west or west-northwest and plunge to the east (Figure 2). The anticlines generally have larger plunge angles than the synclines by 20° to 40° so that the syncline and anticline axes diverge to the west. The axial surfaces of these folds typically dip steeply to the south

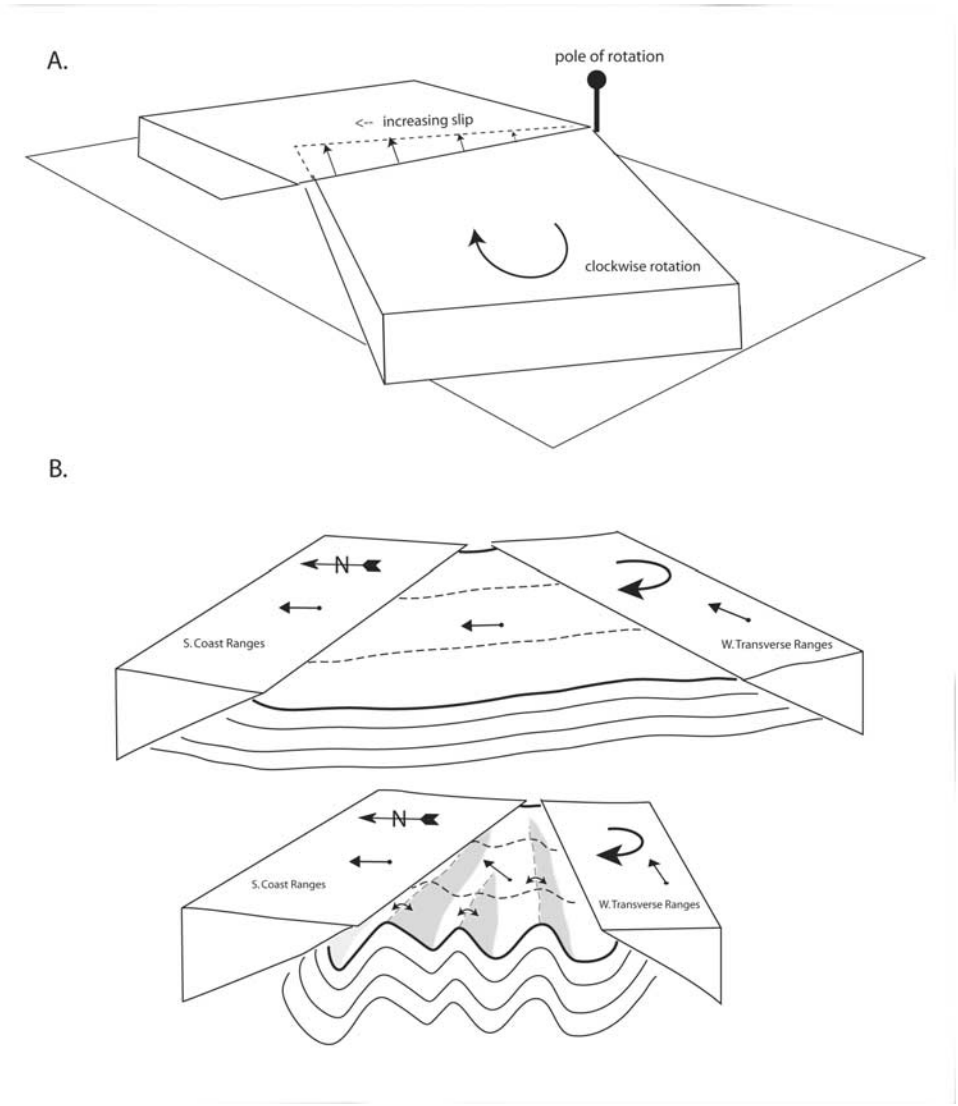

Figure 8. Diagram illustrating vertical axis rotation by (a) reverse faulting and (b) folding. Rotations of paleomagnetic vectors are shown schematically. Note that anticlines plunge toward axis of rotation.

except near the WBP-PM fault where they are overturned and dip to the north. Some map-scale folds trend in a more northwest direction. I interpret these northwest trending folds to be older structures that were rotated clockwise from original east-west orientations because they are locally refolded by younger west trending folds and are typically bent parallel to or truncated by the west striking faults (Figure 2). The boundary zone widens from about 1 km in the east to 20 km in the west where a larger number of folds are present. Unfolding the Miocene and Eocene stratigraphic horizons across the zone shows that differential shortening has occurred, with approximately 18 km of shortening in the west and 4.3 km in the east. The westward increase in shortening in the boundary zone results in a differential rotation of 20° between the northern and southern edges due to folding alone. This rotational folding is consistent with the observation that anticline and syncline axes in the zone diverge to the west away from the pole of rotation (Figure 8).

4.3. Timing of Deformation

[24] Unconformities in the Miocene and younger rocks within the rotation boundary zone and offset units along the major faults indicate than deformation began in middle Miocene time and continued through late Pliocene time. The base of the middle Miocene Monterey Formation in the boundary zone lies unconformably on Late Cretaceous through early Miocene rocks. The timing of this unconformity (~18 Ma [*Fritsche*, 1988; *Vedder and Stanley*, 2001]) roughly coincides with the onset of rotation at about 18 Ma [*Luyendyk*, 1991]. A Luisian foraminifera stage (16 to 14 Ma) unconformity in marine deposits along the south side of the WBP-PM fault [*Perri and Fritsche*, 1988] indicates that episodes of uplift and

deformation occurred in Miocene time. All the faults in the boundary zone cut or deform Miocene rocks and are interpreted to be active during all or the later stages of rotation of the WTR. The WBP-PM fault and the Santa Ynez fault also cut younger units and have geomorphic evidence, such as linear mountain fronts and valleys, fault scarps, and 1.3 to 2 km high mountain ranges in their hanging walls, that suggest Quaternary slip.

5. Interpretations and Discussion

5.1. Rotational Deformation Along the Boundary

[25] The westward increase in shortening exhibited by the faults and folds that make up the boundary zone provide a mechanism for differential rotation between the WTR and the southern Coast Ranges (Figure 8). The wedge-shaped zone was closed in a fan-like fashion as the WTR rotated clockwise around a pole to the east. Differential shortening was most likely accommodated by folding in the earlier stages of rotation and was largely replaced by reverse faulting in the later stages. The early folds have been rotated and are refolded by younger east-west trending folds or truncated by faults. The WBP-PM fault and the Santa Ynez fault truncate all the structures in the boundary zone as well as northwest trending structures of the southern Coast Ranges. I interpret these faults to be the dominant structures in the zone due to significant contrasts across the faults in structural orientations and paleomagnetic declinations.

[26] Restoration of folding in the boundary zone results in 20° of rotation. The westward increase in dip-slip displacement along the reverse faults must also result in rotation. However, estimates of rotation across the two largest faults in the boundary zone, the WBP-PM fault and the Santa Ynez fault, must be inferred from the observed paleomagnetic contrasts due to the impossibility of determining quantitative displacement along these faults. Contrasts in paleomagnetic declinations suggest approximately 30° to 45° of rotation across the WBP-PM fault and 15° to 20° across the Santa Ynez fault. I emphasize that these numbers must be regarded as rough estimates until additional data are available to precisely define the amount of rotation across these faults.

[27] Deformation in the boundary zone differs in both style and age from structures within the rotated domain to the south. Although the entire WTR has experienced north-south directed shortening, the structures within the WTR do not exhibit a westward increase in shortening as seen along the northern boundary and there is significantly less shortening by folding across the WTR (average of about 10% [*Sorlien et al.*, 2000]). Within the WTR, fault displacements are greater in the east along the San Cayetano and Oak Ridge faults (approximately 5 to 7 km on each fault) and decrease slightly to the west in the Santa Barbara Channel [*Sorlien et al.*, 2000]. Displacement along the major structures within the WTR is Pliocene to Quaternary in age and there is no evidence for significant pre-Pliocene shortening [*Yeats*, 1983; *Shaw and Suppe*, 1994], indicating that the observed deformation is primarily younger than the deformation observed in the rotation boundary zone.

5.2. Implications for Regional Models

[28] Much progress has been made by previous investigators toward a kinematic description and explanation of the large vertical axis crustal rotations in southern California. The results of this study contribute to our understanding of this process by providing additional data and links to structural constraints that refine the regional models and reconstructions. Previous rotation models and tectonic reconstructions of southern California have inferred the northern boundary of the rotated WTR domain to be either the Santa Ynez fault or the Big Pine fault, exhibiting primarily left-lateral strike-slip displacement. The paleomagnetic data presented here show that a change from rotated to nonrotated crust does not occur across a single fault. Instead, the observed contrasts are distributed across a transition zone characterized by reverse faults and folds between, and including, the WBP-PM fault and the Santa Ynez fault. This observation requires revision of the existing models along the rotation boundaries. Specifically, I infer that the space problems (overlaps and holes) predicted at the rotation boundaries in the geometric models [e.g., *Luyendyk*, 1991; *Dickinson*, 1996] are alleviated by dip-slip faulting and folding with shortening amounts that vary along strike. A key aspect of the *Luyendyk* [1991] model is that nonrotated crust north of the WTR made space for the rotating block by sliding to the northwest along right-lateral oblique-slip faults. This would create holes or overlaps where the right-lateral faults intersect the rotation boundary and predicts variable amounts of shortening or extension along the rotation boundary. This mechanism is supported by observed right-lateral slip along the northwest faults of the southern Coast Ranges and the observation that estimates of dip-slip displacement along the WBP-PM fault change sharply where faults from the southern Coast Ranges intersect the fault. However, most of the right-lateral displacement along the northwest trending faults of the southern Coast Ranges occurred before the middle Miocene. For example, *Dibblee* [1976] reported a total of 43 km right-lateral slip on the Rinconada (Nacimiento) fault, but *Yaldezian et al.* [1983] presented evidence for a maximum of 6 km of right-lateral slip on the fault since middle Miocene time. Similarly, the only evidence for right-lateral slip on the Ozena fault is reported to be a maximum of 3.7 km since 19 Ma by *Yeats et al.* [1989], who linked the fault to the subsurface Russell fault to the north. I suggest that although right-lateral displacement along faults in the southern Coast Ranges did facilitate some rotation, it was not as significant as required by previous geometric models. The available data indicate that thrusting of the southern Coast Ranges over the rotation boundary, as observed in this study, and shortening within the southern Coast Ranges, was the dominant form of deformation along the northern edge of the boundary during rotation.

[29] The model of rotation boundary mechanics presented here may also apply to other areas of vertical axis rotation. For example, strike-slip faults have been inferred to delineate the boundaries of other rotated domains in southern California, such as the northeastern Mojave Desert [*Schermer et al.*, 1996] and the eastern Transverse Ranges [*Terres*, 1984; *Luyendyk*, 1991]. The results of this study suggest that these inferred boundaries may exhibit different kinematics than previously supposed.

6. Conclusion

[30] Synthesis of paleomagnetic data reported here and previously reported data better constrains the location and spatial extent of a rotation boundary in southern California. Paleomagnetic contrasts at the northern edge of the WTR occur across a zone of reverse faults and folds bounded by the WBP-PM fault on the north and the Santa Ynez fault on the south. Increased amounts of shortening to the west allowed this boundary zone to absorb differential rotation between the WTR and the nonrotated southern Coast Ranges to the north. The results of this study provide a description of rotation boundary kinematics based on field observations and suggest that dip-slip faulting is the dominant form of deformation at the boundaries between rotated and nonrotated crust.

Appendix A: The Big Pine Fault

[31] A complete description of the kinematic history and structural framework of the previously named Big Pine fault is beyond the scope of this paper and will be addressed elsewhere. However, in this appendix I present some of the key lines of evidence that question the interpretation of 14 km of Quaternary left-lateral strike-slip on the Big Pine fault.

[32] *Hill and Dibblee* [1953] first interpreted the Big Pine fault to exhibit left-lateral strike-slip offset based on the following arguments: (1) Oblique-slip striations and reversals in dip and throw along the fault, which led them to interpret primarily strike-slip displacement, (2) left-lateral offset of drainages along the fault, (3) east-west trending drag folds adjacent to the fault, (4) left-lateral offset of the Piedra Blanca syncline and San Guillermo fault on the south from the Madulce syncline and Ozena fault on the north, (5) offset of Miocene sedimentary rocks in the Cuyama Badlands from those in Lockwood Valley, and (6) a well that penetrated granite north of the fault that is exposed farther to the east on the south side of the fault.

[33] The results of this study do not agree with the previous interpretation. The reversals in dip and throw observed by Hill and Dibblee occur in two locations: (1) where the Big Pine fault intersects the Pine Mountain fault and (2) where the Big Pine fault intersects the San Guillermo fault. The abrupt differences observed at the first location are explained by the data and interpretations presented here that the western Big Pine fault is continuous with Pine Mountain fault, which truncates the eastern Big Pine fault. Data and new mapping presented by *Minor* [1999] show that the south dipping eastern Big Pine fault, at the southern edge of the Cuyama Badlands, is continuous with the south dipping San Guillermo fault and does not connect to the major fault present along the north edge of Lockwood Valley. This observation explains the sharp changes observed at the second location and contradicts the previous interpretation that the San Guillermo fault is the left-laterally offset equivalent of the Ozena fault. The current distribution of Miocene terrestrial units in the Cuyama Badlands along the east side of the Ozena fault and in Lockwood Valley mentioned by *Hill and Dibblee* [1953] does not necessitate left-lateral displacement. These rocks are also present in the hanging wall on the west side of the San Guillermo fault as well as on Mount Pinos to the north of Lockwood Valley. The present-day distribution of these rocks, and the orientations of the folds that deform them, are better explained by reverse displacement on the intervening faults. In addition, the presence of the overlying Pliocene Quatal formation on both sides of the Big Pine fault at the southern edge of the Cuyama Badlands indicates that there has been no significant lateral displacement since these rocks were deposited. Deflection of streams that cross the Big Pine fault is not consistent and does not necessitate left-lateral strike slip on the fault. Streams are deflected in both a right-lateral and left-lateral sense, most are not deflected at all, and similar pronounced deflections are commonly observed in the surrounding region where no faults exist. Apparent offset of the Madulce and Piedra Blanca synclines across the Big Pine fault is suggestive of left-lateral displacement. However, smaller folds and faults that parallel these synclines do not match up across the fault, making a correlation based on structural correlations difficult to justify. In addition, these synclines deform Eocene rocks and are unconformably overlain by Miocene strata, indicating that the folds were formed before Miocene time. It is therefore possible that, if these synclines are the same, the apparent left-lateral offset may have occurred along an older structure. This older structure may be hidden or reactivated by the reverse faults that now truncate the synclines and have refolded the Piedra Blanca syncline, which plunges northward as it nears the Big Pine fault.

[34] The data presented here show that the Big Pine fault is not a laterally continuous structure, but rather an alignment of three separate faults. This calls for a reevaluation of the reported left-lateral offsets along the fault and may hold significant implications for tectonic reconstructions of southern California.

[35] **Acknowledgments.** This paper is an outcome of the author's Ph.D. research, during which Art Sylvester and Bruce Luyendyk were a tremendous help. Paleomagnetic data were processed at the California Institute of Technology, and Joe Kirschvink is gratefully acknowledged for his assistance. The manuscript benefited greatly from reviews by B. Dickinson, T. Ross, J. Fryxell, L. Brown, J. Geissman, and G. Dupont-Nivet. Funding for this research was provided by the U.S. Geological Survey and fellowships from the University of California, Richard Migues, and the American Federation of Mineralogical Societies.

References

Arason, P., and S. Levi (1990), Models of inclination shallowing during sediment compaction, *J. Geophys. Res.*, *95*, 4481–4499.

Atwater, T. (1989), Plate tectonic history of the northeast Pacific and western North America, in *The Geology of North America*, vol. N, *The Eastern Pacific Ocean and Hawaii*, edited by E. L. Winterer et al., pp. 21–71, Geol. Soc. of Am., Boulder, Colo.

Beck, M. E., Jr. (1980), Paleomagnetic record of plate-margin tectonic processes along the western edge of North America, *J. Geophys. Res.*, *85*(B12), 7115–7131.

Calderone, G. J., R. F. Butler, and G. D. Acton (1990), Paleomagnetism of middle Miocene volcanic rocks in the Mojave-Sonora Desert region of western Arizona and southeastern California, *J. Geophys. Res.*, *95*, 625–647.

Champion, D. E., D. G. Howell, and C. S. Gromme (1984), Paleomagnetic and geologic data indicating 2500 km of northward displacement for the Salinian and related terranes, California, *J. Geophys. Res.*, *89*, 7736–7752.

Crouch, J. (1979), Neogene tectonic evolution of the California Continental Borderland and western Transverse Ranges, *Geol. Soc. Am. Bull., Part 1*, *90*, 338–345.

Crouch, J., and J. Suppe (1993), Late Cenozoic tectonic evolution of the Los Angeles basin and inner California borderland: A model for core complex-like crustal extension, *Geol. Soc. Am. Bull.*, *105*, 1415–1434.

Demarest, H. H., Jr. (1983), Error analysis for the determination of tectonic rotation from paleomagnetic data, *J. Geophys. Res.*, *88*, 4321–4328.

Dibblee, T., Jr. (1976), Rinconada and related faults in the southern Coast Ranges, California, and their tectonic significance, *U.S. Geol. Surv. Prof. Pap.*, *981*.

Dibblee, T., Jr. (1982), Regional Geology of the Transverse Ranges Province of southern California, in *Geology and Mineral Wealth of the California Transverse Ranges*, edited by D. L. Fife and J. A. Minch, pp. 7–26, South Coast Geol. Soc., Santa Ana, Calif.

Dibblee, T. W. (1985), Geologic map of the Wheeler Springs quadrangle, Ventura County, California, scale 1:24000, Dibblee Geol. Found., Camarillo, Calif.

Dibblee, T. W., and H. E. Ehrenspeck (Eds.) (1986), Geologic map of the Little Pine Mountain quadrangle, Santa Barbara County, California, scale 1:24000, Dibblee Geol. Found., Camarillo, Calif.

Dibblee, T. W., and H. E. Ehrenspeck (Eds.) (1987a), Geologic map of the San Marcos Pass quadrangle, Santa Barbara County, California, scale 1:24000, Dibblee Geol. Found., Camarillo, Calif.

Dibblee, T. W., , and H. E. Ehrenspeck (Eds.) (1987b), Geologic map of the Lake Cachuma quadrangle, Santa Barbara County, California, scale 1:24000, Dibblee Geol. Found., Camarillo, Calif.

Dibblee, T. W., and H. E. Ehrenspeck (Eds.) (1987c), Geologic map of the Lion Canyon quadrangle, Ventura County, California, scale 1:24000, Dibblee Geol. Found., Camarillo, Calif.

Dibblee, T. W., and H. E. Ehrenspeck (Eds.) (1988), Geologic map of the Santa Ynez and Tajiguas quadrangles, Santa Barbara County, California, scale 1:24000, Dibblee Geol. Found., Camarillo, Calif.

Dibblee, T. W., and H. E. Ehrenspeck (Eds.) (1996a), Geologic map of the Devils Heart Peak quadrangle, Ventura County, California, scale 1:24000, Dibblee Geol. Found., Camarillo, Calif.

Dibblee, T. W., and H. E. Ehrenspeck (Eds.) (1996b), Geologic map of the TopaTopa Mountains quadrangle, Ventura County, California, scale 1:24000, Dibblee Geol. Found., Camarillo, Calif.

Dickinson, W. R. (1996), Kinematics of transrotational tectonism in the California Transverse Ranges and its contribution to cumulative slip along the San Andreas Transform Fault System, *Spec. Pap. Geol. Soc. Am.*, *305*, 46 pp.

Diehl, J. F., M. E. Beck, S. Beske-Diehl, D. Jacobson, and B. C. Hearn (1983), Paleomagnetism of the Late Cretaceous–early Tertiary north-central Montana alkalic province, *J. Geophys. Res.*, *12*, 10,593–10,609.

Edwards, L. N. (1971), Geology of the Vaqueros and Rincon formations, Santa Barbara embayment, California, Ph.D. thesis, Univ. of Calif., Santa Barbara.

Fritsche, A. E. (1988), Origin and paleogeographic development of the Tertiary Cuyama depositonal basin, southern California, in *Tertiary Tectonics and Sedimentation in the Cuyama Basin, San Luis Obispo, Santa Barbara, and Ventura Counties, California*, *Publ. 59*, edited by W. Bazeley, pp. 159–162, Pac. Sect. Soc. for Sediment. Geol., Los Angeles, Calif.

Gordon, S. A. (1978), Relations among the Santa Ynez, Pine Mountain, Agua Blanca, and Cobblestone Mountain faults, Transverse Ranges, California, M.A. thesis, Univ. of Calif., Santa Barbara.

Halls, H. C. (1976), A least-squares method to find a remanence direction from converging remagnetization circles, *Geophys. J. R. Astron. Soc.*, *45*, 297–304.

Hamilton, W. (1978), Mezosoic tectonics of the western United States, in *Mesozoic Paleogeography of the Western United States, Pacific Coast Paleogeography Symposium 2, April 26, 1978*, edited by D. G. Howell and K. A. McDougall, pp. 33–70, Pac. Sect., Soc. for Sediment. Geol., Los Angeles, Calif.

Hill, M. L., and T. W. Dibblee (1953), San Andreas, Garlock, and Big Pine faults, California, *Geol. Soc. Am. Bull.*, *64*, 443–458.

Hoffman, K. A., and R. Day (1978), Separation of multi-component NRM: A general method, *Earth Planet. Sci. Lett.*, *40*(3), 433–438.

Hornafius, J. S. (1985), Neogene tectonic rotation of the Santa Ynez Range, western Transverse Ranges, California, suggested by paleomagnetic investigation of the Monterey Formation, *J. Geophys. Res.*, *90*, 12,503–12,522.

Hornafius, J., B. Luyendyk, R. Terres, and M. Kamerling (1986), Timing and extent of Neogene tectonic rotation in the western Transverse Ranges, California, *Geol. Soc. Am. Bull.*, *97*, 1476–1487.

Jennings, C. H., R. G. Strand, and T. H. Rogers (1977), Geologic map of California, scale 1:750000, 1 sheet, State of Calif. Dep. of Conserv., Sacramento.

Jones, D. L., M. C. Blake Jr., and C. Rangin (1976), The four Jurassic belts of northern California and their significance to the geology of the southern California borderland, in *Aspects of the Geologic History of the California Continental Borderland*, *Misc. Publ. 24*, edited by D. G. Howell, pp. 343–362, Pac. Sect., Am. Assoc. of Pet. Geol., Los Angeles, Calif.

Kamerling, M., and B. Luyendyk (1979), Tectonic rotation of the Santa Monica Mountains region, western Transverse Ranges, California, suggested by paleomagnetic vectors, *Geol. Soc. Am. Bull.*, *90*, 331–337.

Kamerling, M., and B. Luyendyk (1985), Paleomagnetism and Neogene tectonics of the northern Channel Islands, California, *J. Geophys. Res.*, *90*, 12,485–12,502.

Kirschvink, J. L. (1980), The least-squares line and plane and the analysis of palaeomagnetic data, *Geophys. J. R. Astron. Soc.*, *62*, 699–718.

Liddicoat, J. (1990), Tectonic rotation of the Santa Ynez Range, California, recorded in the Sespe Formation, *Geophys. J. Int.*, *102*, 739–745.

Liddicoat, J. (2001), Paleomagnetism of the Sespe Formation (Eocene-Oligocene), Ventura and Santa Barbara counties, California, in *Magnetic Stratigraphy of the Pacific Coast Cenozoic*, *Publ. 91*, edited by D. R. Prothero, Pac. Sect. Soc. for Sediment. Geol., Los Angeles, 144–153.

Link, M. H. (1971), Sedimentology and environmental analysis of the Matilija Sandstone north of the Santa Ynez fault, Santa Barbara County, California, M.A. thesis, Univ. of Calif., Santa Barbara.

Lonsdale, P. (1991), Structural patterns of the Pacific floor offshore of Peninsular California, in *Gulf and Peninsula Province of the Californias*, edited by J. P. Dauphin and B. T. Simoneit, *AAPG Mem.*, *47*, 87–125.

Lund, S. P., D. J. Bottjer, K. J. Whidden, J. E. Powers, and M. C. Steele (1991), Paleomagnetic evidence for Paleogene terrane displacements and accretion in southern California, *Eocene Geological History, San Diego Region*, edited by P. L. Abbott and J. A. May, pp. 99–106, Pac. Sect. Soc. for Sediment. Geol., Los Angeles, Calif.

Luyendyk, B. (1991), A model for Neogene crustal rotations, transtension, and transpression in southern California, *Geol. Soc. Am. Bull.*, *103*, 1528–1536.

Luyendyk, B., M. Kamerling, and R. Terres (1980), Geometric model for Neogene crustal rotations in southern California, *Geol. Soc. Am. Bull.*, *91*, 211–217.

Luyendyk, B. P., M. J. Kamerling, R. R. Terres, and J. S. Hornafius (1985), Simple shear of southern California during Neogene time suggested by paleomagnetic declinations, *J. Geophys. Res.*, *90*, 12,454–12,466.

McCracken, W. A. (1972), Paleocurrents and petrology of Sespe sandstones and conglomerates, Ventura basin, California, Ph.D. thesis, 192 pp., Stanford Univ., Stanford, Calif.

McCulloh, T. H. (1981), Middle Tertiary laumontite isograd offset 37 km by left-lateral strike-slip on the Santa Ynez fault, California, *AAPG Bull.*, *65*, 956.

McElhinny, M. W., and P. L. McFadden (2000), *Paleomagnetism: Continents and Oceans*, 386 pp., Elsevier, New York.

McFadden, P. L., and M. W. McElhinny (1988), The combined analysis of remagnetization circles and direct observations in paleomagnetism, *Earth Planet. Sci. Lett.*, *87*, 161–172.

McWilliams, M. O., and D. G. Howell (1982), Exotic terranes of western California, *Nature*, *297*, 215–217.

Minor, S. A. (1999), Preliminary geologic map of the San Guillermo Mountain quadrangle, Ventura County, California, *U.S. Geol. Surv. Open File Rep., 99-032*.

Nicholson, C., C. Sorlien, T. Atwater, C. Crowell, and B. Luyendyk (1994), Microplate capture, rotation of the western Transverse Ranges, and initiation of the San Andreas transform as a low-angle fault system, *Geology*, *22*, 491–495.

Onderdonk, N. W. (2003), Geometry and kinematics of structures that accommodated large-magnitude differential vertical- axis rotation of the western Transverse Ranges, southern California, Ph.D. thesis, 96 pp., Univ. of Calif., Santa Barbara.

Perri, M. L., and A. E. Fritsche (1988), Stratigraphy and depositonal environments of the Miocene Branch Canyon Formation in the Sierra Madre, Caliente Range, and Sespe Creek areas, California, in *Tertiary Tectonics and Sedimentation in the Cuyama Basin, San Luis Obispo, Santa Barbara, and Ventura Counties, California*, *Publ. 59*, edited by W. Bazeley, pp. 87–96, Pac. Sect., Soc. for Sediment. Geol., Los Angeles, Calif.

Prothero, D. R., and J. R. Britt (1998), Magnetic stratigraphy and tectonic rotation of the Middle Eocene Matilija Sandstone and Cozy Dell Shale, Ventura County, California: Implications for sequence stratigraphic correlations, *Earth Planet. Sci. Lett.*, *168*, 261–273.

Schermer, E. R., B. P. Luyendyk, and S. Cisowski (1996), Late Cenozoic structure and tectonics of

the northern Mojave Desert, *Tectonics*, *15*, 905–932.

Shaw, J. H., and J. Suppe (1994), Active faulting and growth folding in the eastern Santa Barbara Channel, California, *Geol. Soc. Am. Bull.*, *106*, 607–626.

Sorlien, C., J. Gratier, B. Luyendyk, J. Hornafius, and T. Hopps (2000), Map restoration of folded and faulted late Cenozoic strata across the Oaks Ridge fault, onshore and offshore Ventura basin, California, *Geol. Soc. Am. Bull.*, *112*, 1080–1090.

Sylvester, A. G., and A. C. Darrow (1979), Structure and neotectonics of the western Santa Ynez fault system in southern California, *Tectonophysics*, *52*, 389–405.

Terres, R. R. (1984), Paleomagnetism and tectonics of the central and eastern Transverse Ranges, southern California, Ph.D. thesis, 325 pp., Univ. of Calif., Santa Barbara.

Up De Graff, J. E., and B. P. Luyendyk (1989), Gravity study of the boundary between the western Transverse Ranges and Santa Maria Basin, California, *J. Geophys. Res.*, *94*, 1817–1825.

Vedder, J. G., and R. G. Stanley (2001), Geologic map and digital database of the San Rafael Mountain 7.5-minute Quadrangle, Santa Barbara County, California, *U.S. Geol. Surv. Open File Rep., 01-290*.

Whidden, K. J. (1994), Paleogeography of the southern California forearc basin in the Late Cretaceous and early Paleogene: Evidence from paleomagnetism and carbonate facies analysis, Ph.D. thesis, Univ. of South. Calif., Los Angeles.

Yaldezian, J. G., S. J. Popelar, and A. E. Fritsche (1983), Movement on the Nacimiento Fault in northern Santa Barbara County, California, in *Tectonics and Sedimentation Along Faults of the San Andreas System*, edited by D. W. Anderson and M. J. Rymer, pp. 11–15, Pac. Sect. Soc. for Sediment. Geol., Los Angeles, Calif.

Yeats, R. S. (1983), Large-scale Quaternary detachments in the Ventura basin, southern California, *J. Geophys. Res.*, *88*, 569–583.

Yeats, R. S., M. R. Cole, W. R. Merschat, and R. M. Parsley (1974), Poway fan and submarine cone and rifting of the inner southern California borderland, *Geol. Soc. Am. Bull.*, *85*, 293–302.

Yeats, R. S., J. A. Calhoun, B. B. Nevins, H. F. Schwing, and H. M. Spitz (1989), The Russell fault: An early strike slip fault of the California Coast Ranges, *AAPG Bull.*, *73*, 1089–1102.

N. W. Onderdonk, Physics of Geological Processes, University of Oslo, P.O. Box 1048 Blindern, N-0316 Oslo, Norway. (nate.onderdonk@fys.uio.no)